Editors' Suggestion

Fluxonium: An Alternative Qubit Platform for High-Fidelity Operations

Feng Bao,[1] Hao Deng,[1] Dawei Ding,[2] Ran Gao,[1] Xun Gao,[2] Cupjin Huang,[2] Xun Jiang,[1] Hsiang-Sheng Ku,[1] Zhisheng Li,[1] Xizheng Ma,[1] Xiaotong Ni,[1] Jin Qin,[1] Zhijun Song,[1] Hantao Sun,[1] Chengchun Tang,[1] Tenghui Wang,[1] Feng Wu,[1] Tian Xia,[1] Wenlong Yu,[1] Fang Zhang,[2] Gengyan Zhang,[1] Xiaohang Zhang,[1] Jingwei Zhou,[1] Xing Zhu,[1] Yaoyun Shi,[2,*] Jianxin Chen,[2] Hui-Hai Zhao,[3] and Chunqing Deng[1,†]

[1]*Alibaba Quantum Laboratory, Alibaba Group, Hangzhou, Zhejiang 311121, People's Republic of China*

[2]*Alibaba Quantum Laboratory, Alibaba Group USA, Bellevue, Washington, D.C. 98004, USA*

[3]*Alibaba Quantum Laboratory, Alibaba Group, Beijing 100102, People's Republic of China*

(Received 12 January 2022; accepted 1 June 2022; published 28 June 2022)

Superconducting qubits provide a promising path toward building large-scale quantum computers. The simple and robust transmon qubit has been the leading platform, achieving multiple milestones. However, fault-tolerant quantum computing calls for qubit operations at error rates significantly lower than those exhibited in the state of the art. Consequently, alternative superconducting qubits with better error protection have attracted increasing interest. Among them, fluxonium is a particularly promising candidate, featuring large anharmonicity and long coherence times. Here, we engineer a fluxonium-based quantum processor that integrates high qubit coherence, fast frequency tunability, and individual-qubit addressability for reset, readout, and gates. With simple and fast gate schemes, we achieve an average single-qubit gate fidelity of 99.97% and a two-qubit gate fidelity of up to 99.72%. This performance is comparable to the highest values reported in the literature of superconducting circuits. Thus our work, within the realm of superconducting qubits, reveals an alternative qubit platform that is competitive with the transmon system.

DOI: 10.1103/PhysRevLett.129.010502

The performance of a quantum processor, characterized by the fidelity of its operations, is confined by the ratio between the operation time and the decoherence times of the qubits. Early superconducting qubits, such as the Cooper-pair box qubit [1] and flux qubit [2], suffer from extremely fast dephasing rates due to their large susceptibility to charge or flux noises. By shunting the Josephson junction with a large capacitor, the transmon qubit [3] protects against charge-noise-induced dephasing, leading to its exceptional success in the past decade [4–6]. However, this protection comes at the cost of a reduced anharmonicity. Although advanced qubit control schemes [7,8] and frequency-selective processor architectures [9,10] can be adopted to circumvent the speed limit of gate operations imposed by the weak anharmonicity, the leakage to noncomputational states in such fast operations remains a challenge to quantum error correction [11,12]. Furthermore, transmon qubits still suffer from relaxation due to material imperfections such as dielectric loss [13,14], which can be challenging to improve [15].

In contrast, by shunting the Josephson junction with a large linear inductor, fluxonium [16] protects against low-frequency charge fluctuations while retaining a large anharmonicity. Compared with a flux qubit, the flux-noise-induced dephasing of fluxonium is suppressed by the large inductor, enabling operations away from its flux insensitive point. Additionally, fluxonium can be operated at a qubit frequency $\lesssim 1$ GHz where energy relaxation is largely reduced due to its suppressed coupling to dielectric loss. Indeed, isolated single fluxonium qubits have demonstrated long coherence times ranging from a few hundred microseconds to a millisecond [17–19].

Despite these intuitive advantages, combining high coherence with fast operations, including gates, reset, and readout, in a single high-fidelity fluxonium processor remains challenging. First, the large shunt inductor, composed of more than a hundred Josephson junctions, is susceptible to additional decoherence sources. The best fluxonium qubits achieve an intrinsic loss tangent of approximately 10^{-6} [17,19], defined as the qubit decay rate divided by its frequency, an order of magnitude worse than that achieved in the state-of-the-art transmon [20,21]. Therefore, fluxonium qubits need to be operated at a much lower frequency than a typical transmon qubit to reach a comparable coherence time. Second, the suppression of energy relaxation from dielectric loss at a low qubit frequency often leads to a weaker qubit-qubit interaction and slowdown of the two-qubit gate speed in the widely adopted capacitive coupling scheme. Consequently, two-qubit gate demonstrations [22,23] thus far have been limited to microwave-activated schemes that exploit dynamics outside the computational space and thus are limited by the relatively short-lived higher excited states.

Here, we consider a two-qubit system with direct capacitive coupling for gates only involving levels within the computational space. We choose the circuit parameters

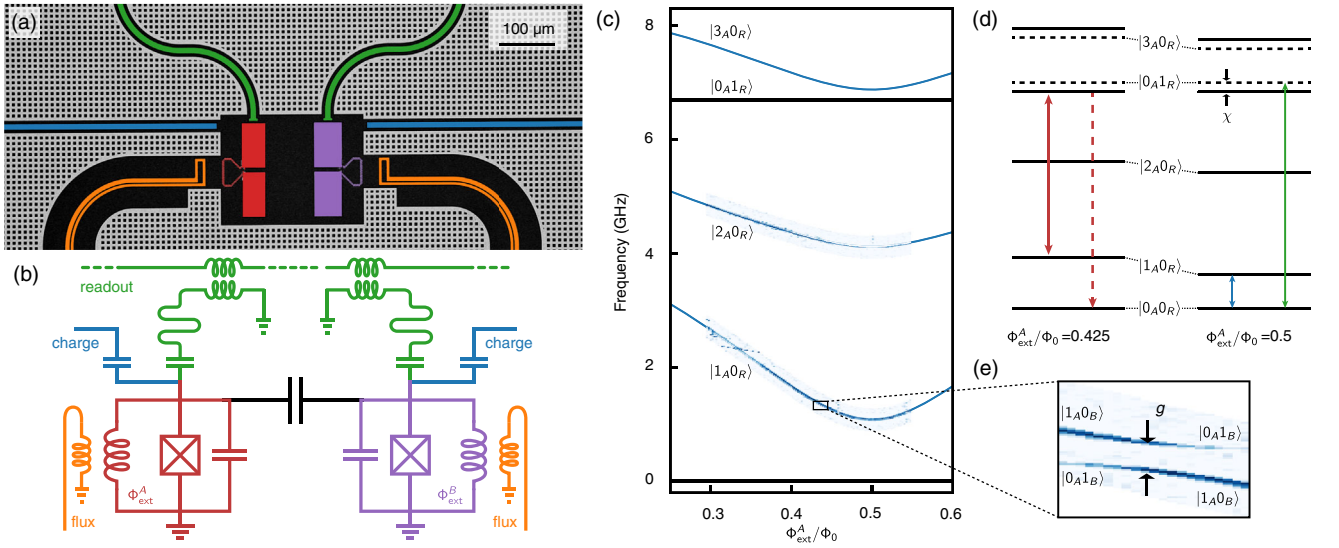

FIG. 1. (a) False-colored optical image of the fluxonium processor made of aluminum (colored and white) on a silicon substrate (black). The colored metals correspond to the circuit components in the schematic shown in (b). The two qubits Q_A (red) and Q_B (purple), each consisting of a superconducting loop made from Josephson junctions [25] and a shunting capacitor, couple to each other through direct capacitive coupling. Individually, qubits are driven through capacitively coupled microwave charge lines (blue), frequency control is achieved through inductively coupled flux lines (orange), and readout is achieved by measuring the resonant frequency shift of the microwave resonators (green). (c) Spectroscopy of Q_A as a function of the external flux through the qubit loop. Lines indicate a fit to the spectrum of the qubit model. (d) Energy diagrams of the qubit-resonator coupled system for Q_A at the $\Phi^A_{\rm ext} = 0.5\Phi_0$ flux sweet spot and $\Phi^A_{\rm ext} = 0.425\Phi_0$ where the reset is performed. Microwave irradiations used for qubit excitation (blue), reset (red), and readout (green) are shown as arrows. Dashed lines indicate levels without qubit-resonator interaction. (e) two-qubit spectroscopy with the transition frequency of Q_A sweeping across that of Q_B idled at the flux sweet spot.

to minimize the two-qubit gate error by balancing two primary error sources: decoherence and stray ZZ interactions [24]. In particular, the decoherence error can be reduced by decreasing the qubit frequency and increasing the coupling strength for a fixed gate time at the expense of increasing ZZ errors arising from the strong interactions between the computational levels and higher excited states. For an iSWAP gate, we find the best gate fidelity at the qubit frequencies around 1.2 GHz and coupling strength corresponding to a gate time of approximately 40–50 ns, assuming dielectric loss at the level of 10^{-6}.

We perform meticulous engineering to combine high-coherence fluxonium qubits with a planar integrated circuit that is similar to a scalable transmon processor [48]. As shown in Figs. 1(a) and 1(b), our processor consists of two capacitively coupled fluxonium qubits Q_A and Q_B in a circuit quantum electrodynamics architecture [49]. The qubits can be addressed individually using microwave signals to perform independent excitation through charge lines and dispersive readout through dedicated quarter-wave resonators. Using on-chip flux lines, we independently control the frequency of each qubit by imposing a flux $\Phi^\alpha_{\rm ext}$ ($\alpha = A$ or B) that threads its qubit loop, formed between the phase-slip Josephson junction and the linear inductor consisting of an array of 100 Josephson junctions. Importantly, the flux lines with DC-300 MHz bandwidth allow for rapid tuning of the qubit frequency. This enables one to operate the qubit at different frequencies for reset, gates, and readout for best performance as well as two-qubit swapping operations that remain entirely within the computational space at a theoretically maximum speed limited by the qubit-qubit coupling strength.

The measured qubit spectrum versus the flux bias of Q_A and its fit to the fluxonium model is shown in Fig. 1(c) [25]. At $\Phi^A_{\rm ext} = \Phi_0/2$, the qubit frequency, defined as the transition frequency between the ground and first excited states, is first-order insensitive to flux noise (known as the flux sweet spot) and $\omega_{10} = 2\pi \times 1.09$ GHz. The transition frequency between the first and second excited states is given by $\omega_{21} = 2\pi \times 3.02$ GHz. The qubit anharmonicity, measured by a quantity defined as $(\omega_{21} - \omega_{10})/\omega_{10}$, is 1.771, one order of magnitude larger than that of a typical transmon qubit. We measure the qubit-qubit coupling strength by probing the flux-dependent spectrum of Q_A with Q_B idled at its flux sweet spot, at a qubit frequency of 1.33 GHz [Fig. 1(e)]. From the level repulsion due to transverse coupling between the states $|1_A0_B\rangle$ and $|0_A1_B\rangle$, where $|k_Al_B\rangle$ denotes the excitation level $k(l)$ for $Q_A(Q_B)$, a spin-exchange interaction strength $g = 2\pi \times 11.2$ MHz is obtained from the minimum size of the energy splitting.

To exploit the large anharmonicity and the first-order protection against the flux noise of fluxonium, we operate the qubits around their $\Phi^A_{\rm ext} = \Phi^B_{\rm ext} = \Phi_0/2$ flux sweet spots. In Fig. 1(d), we show the energy diagram of the

coupled qubit-resonator system for Q_A to explain the resonator-assisted operations, including the readout and reset. The level labeled $|k_A n_R\rangle$ corresponds to a product state with k_A and n_R excitation in the qubit Q_A and in the resonator, respectively. Although the qubit is far detuned from the readout resonator with a resonant frequency $\omega_R = 2\pi \times 6.696$ GHz, a sizable qubit state dependent resonance shift $\chi = 2\pi \times 0.63$ MHz is obtained and can be attributed to the strong coupling and hybridization of the $|3_A 0_R\rangle$ and $|0_A 1_R\rangle$ states [25]. Thus, qubit readout can be achieved by performing homodyne measurements at the resonator frequency. The readout resonator has a photon spontaneous emission rate $\kappa \approx (70\ \text{ns})^{-1}$, which allows for fast readout, and is also used as a damping channel for qubit reset. We note that reset is a necessary operation for fluxonium as the qubit energy $\hbar\omega_{10} \lesssim k_B T$ therefore the first excited state can be thermally populated. We implemented a red-sideband reset similar to Ref. [50], in which the population is first transferred from $|1_A 0_R\rangle$ to $|0_A 1_R\rangle$ and then quickly relaxes to the ground state $|0_A 0_R\rangle$ through resonator emission. Simultaneous to the red-sideband drive, we apply a fast flux pulse to offset the qubit away from the $\Phi^A_{\text{ext}} = \Phi_0/2$ point, lifting the selection rule for this sideband transition. This reset scheme is naturally built in our processor architecture. It is robust in a sense that it requires neither multiple microwave tones nor high-power excitations that could lead to spurious transitions thus is advantageous over the previous schemes [18,50]. After reset, we identified a ground state population of greater than 95% and a readout contrast of 88%. The reset and readout fidelity can be further improved by increasing the sideband transition matrix element with larger flux offset and increasing the readout signal-to-noise ratio with a quantum limited amplifier [51].

The coherence times of the qubits at the flux sweet spots are measured to be $T_1 = 80(57)\ \mu$s and $T_{2,\text{echo}} = 30(17)\ \mu$s for $Q_A(Q_B)$. We also measured the flux dependence of coherence times within a few hundred MHz qubit frequency in the vicinity of the $\Phi^{\alpha}_{\text{ext}} = \Phi_0/2$ point where both T_1 and T_2 nominally have the highest values. The data is consistent with dielectric loss, i.e., relaxation to two-level systems, and dephasing due to low-frequency flux noise [25].

Because of the large anharmonicity and high coherence, we can perform fast, high-fidelity single qubit operations with simple control pulses. Specifically, we pulse on the resonant microwave drives with simple cosine envelopes [25] to rotate the qubit in its Bloch sphere. We calibrate [25] a primary set of gate operations in qubit Q_A, denoted as $\{I, X_\pi, Y_\pi, X_{\pm\pi/2}, Y_{\pm\pi/2}\}$, consisting of 0, π, and $\pi/2$ rotations around two independent axes X and Y, with a fixed gate duration of 10 ns. The fidelity of these primary gates can be characterized using randomized benchmarking (RB) of Clifford operations [52–54] [Fig. 2(a)]. Before every sequence, we initialize the qubit into its ground state by a reset. This measurement extracts an average fidelity of 99.97% across all primary gates [25]. We then further benchmark the fidelity of each specific gate (G) by appending it after every Clifford operation. We find that the fidelities of identity (I) and the $X_{\pi/2}$ gate are 99.99% and 99.98% respectively, in reasonably good agreement with the limit of decoherence [25]. However, the error of the X_π gate, extracted from its 99.96% fidelity, is more than double of that of the $X_{\pi/2}$ gate and thus cannot be explained by decoherence alone.

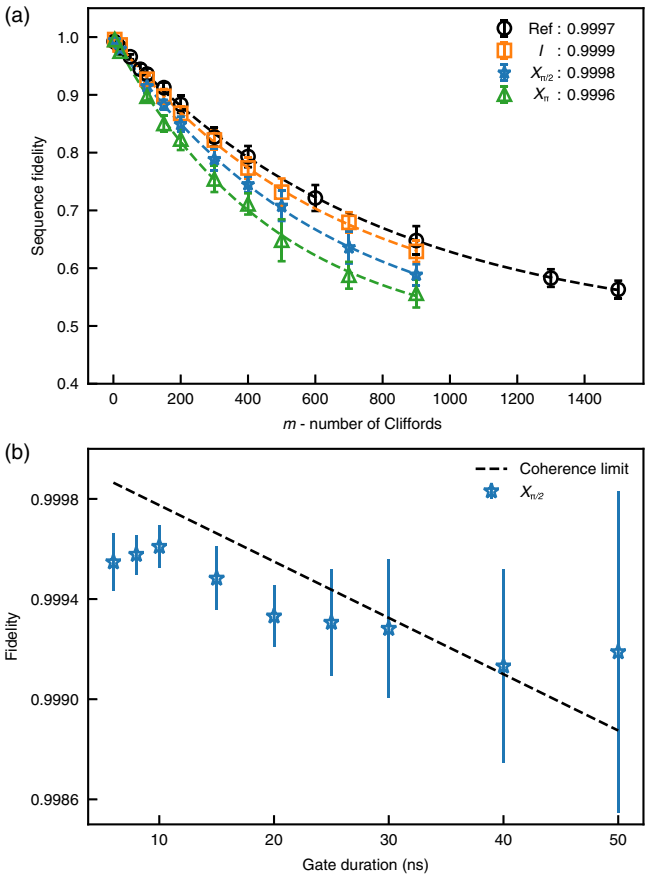

FIG. 2. (a) Sequence fidelities of reference and interleaved RB with sequences of m random Clifford gates. For the fidelity of each value of m, 20 random sequences are used to obtain the average sequence fidelity, and the standard deviation is displayed as error bars. (b) Fidelity of $X_{\pi/2}$ as a function of gate duration. The black dashed line represents the calculated coherence limit.

We next measure the gate fidelity of $X_{\pi/2}$ as a function of the gate duration. A gate with a shorter duration is implemented with a larger amplitude to ensure a fixed $\pi/2$ rotation angle. The experiment is performed on Q_B, and the results are shown in Fig. 2(b). The gate fidelity generally increases with deceasing gate duration and remains close to the coherence limit (black dashed line). We observe no sign of elevated gate error on short gate durations down to 10 ns without employing advanced pulse-shaping techniques such as derivative removal by

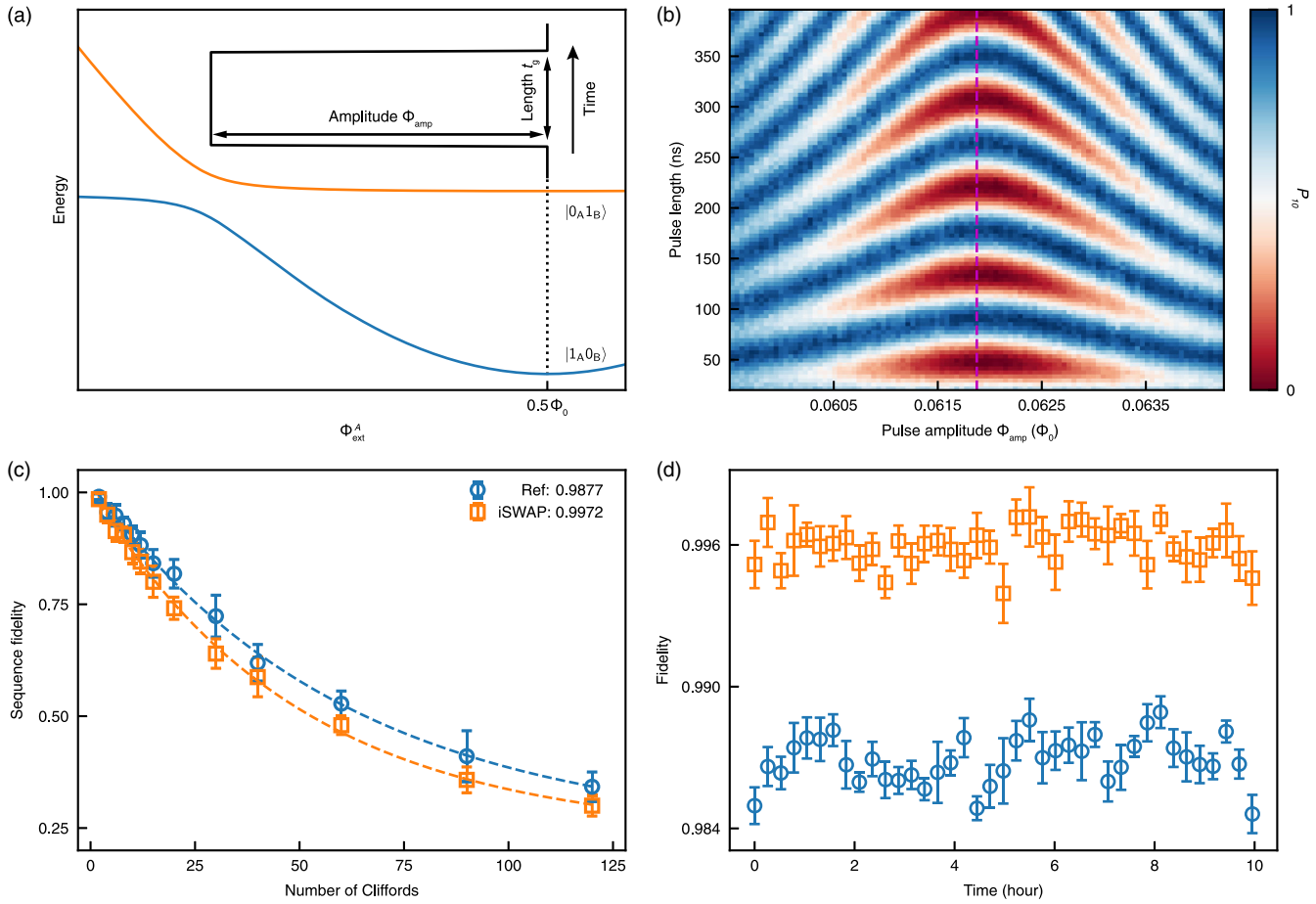

FIG. 3. (a) Schematic of the level structure involving the energy eigenstates $|0_A1_B\rangle$ and $|1_A0_B\rangle$. Insert: the flux control pulse that activates the iSWAP operation. (b) Coherent oscillation of the population between the state $|0_A1_B\rangle$ and $|1_A0_B\rangle$, shown as P_{01} as a function of the pulse amplitude Φ_{amp} and pulse length t_g. The magenta dashed line corresponds to the pulse amplitude where the swapping rate is at the minimum and the system undergoes a complete population exchange from one qubit to the other. (c) Sequence fidelity of Clifford RB and interleaved RB of the iSWAP gate. Each fidelity is obtained from averaging over 10 random sequences. (d) Temporal fluctuation of the fidelities for the two-qubit Clifford gates and the iSWAP gate. The error bars are calculated from the uncertainty of fitting parameters.

adiabatic gate [7]. Using numerical simulations, we find population leakage as low as 10^{-8} at a 10 ns gate duration, enabled entirely by the large anharmonicity of the fluxonium qubit [25]. This shows that the gate fidelity is possibly affected by other sources of imperfections during strong driving, such as heating or pulse distortions [55].

We complement our single-qubit gates with a two-qubit iSWAP gate. The iSWAP gate is performed at the point of avoided level crossing [Fig. 3(a)] due to the direct qubit-qubit interaction. Specifically, after initializing the qubit pair into $|1_A0_B\rangle$, we use the broadband flux line to alter the frequency of qubit Q_A and bring it adiabatically into resonance with qubit Q_B for a duration t_g. Figure 3(b) shows the resulting spin-exchange-like oscillation between the two qubits at a rate $\sqrt{g^2+\Delta^2}$ given by the qubit-qubit coupling strength $g \approx 2\pi \times 11.2$ MHz and the qubit frequency difference Δ set by the flux-pulse amplitude Φ_{amp}. An iSWAP gate is realized at $t_g = 50$ ns and $\Delta = 0$ (magenta dashed line). The fine tuning details of the gate can be found in the Supplemental Material [25]. To characterize the performance of our iSWAP gate, we perform RB as discussed above, but with two-qubit Clifford gates generated by a combination of the iSWAP gate and the single-qubit primary gates, $\{I, X_\pi, Y_\pi, X_{\pm\pi/2}, Y_{\pm\pi/2}\}$. As shown in Fig. 3(c), we find an average fidelity of 98.77% for two-qubit Clifford gates and a fidelity up to 99.72% for the iSWAP gate. In Fig. 3(d), we show the temporal fluctuation of the gate fidelity. In a 10-hour duration, we find an average iSWAP gate fidelity of 99.60%, demonstrating the very good stability of this flux tunable gate. Finally, we analyze the limit of this gate scheme through numerical simulations [25]. We find that 0.05% infidelity can be attributed to control errors due to pulse imprecision and stray qubit-qubit interactions. Importantly, because of the large anharmonicity of the qubit, the stray ZZ interaction strength, measured to be

0.235 MHz, only contributes to approximately 0.03% gate infidelity. Our gate scheme is considerably simpler than the ZZ-free iSWAP with weakly anharmonic qubits which either requires a tunable coupler controlled by an advanced pulse scheme [56] or two different kinds of qubits with opposite-sign anharmonicity [57]. Moreover, the leakage error of our gate scheme is negligible. Instead, our iSWAP gate infidelity is dominated by qubit decoherence, where qubit relaxation and dephasing each contribute 0.06% and 0.26%, respectively, to gate errors.

To summarize, we realize a fluxonium processor with single- and two-qubit gate fidelities comparable to the state of the art in the widely adopted transmon qubits [56,58]. This performance is achieved through simple, fast, and low-leakage gate schemes with fast frequency tunability and individual controls. Importantly, this high-fidelity gate set is demonstrated together with built-in robust reset and readout in a single device, thus fulfilling all the criteria of the physical implementation of quantum computing [59].

The theoretical characteristics of fluxonium and our infidelity analyses lead naturally to an avenue discussed below for further developments. Although the fluxonium coherence times in this Letter have not exceeded those best-reported values, the extracted dielectric loss in our devices is approximately 10^{-6} [25], comparable to the most coherent fluxonium demonstrated thus far [17,19]. We thus anticipate that a significant improvement in qubit coherence can be achieved by lowering the frequency, without the need of further reducing dielectric loss. This coherence enhancement is a result of the suppressed transition matrix element of the charge operator of fluxonium, which inevitably slows down the gates based on capacitive couplings. Inductive couplings, however, do not suffer from the above limitation. We expect that our gate schemes can be applied to strongly inductively coupled and high-coherence fluxonium qubits, leading to even higher fidelity gates as well as other operations. To scale up, tunable couplers [4,60] are a crucial component to maintain high fidelity for parallel operations in a large superconducting circuit. Such schemes are known for inductively coupled flux qubits [61,62], which have essentially the same form of Hamiltonian as fluxonium. Moreover, 3D integration techniques [63] can be adopted for the suppression of on-chip spurious modes and crosstalk while providing more wire routing spaces for a large number of qubits. Therefore, our work not only suggests a viable alternative path for fault tolerance, but one that may eventually outperform transmon, the current mainstream qubit of choice.

We thank all full-time associates at Alibaba Quantum Laboratory for experimental support, and Xin Wan and Shi-Biao Zheng for insightful discussions. Y. S. is indebted to Jeff Zhang for his patience and support, which is indispensable for the team's risk-taking spirit.

*y.shi@alibaba-inc.com
†chunqing.cd@alibaba-inc.com

[1] Y. Nakamura, Y. A. Pashkin, and J. S. Tsai, Nature (London) **398**, 786 (1999).
[2] J. E. Mooij, T. P. Orlando, L. Levitov, L. Tian, C. H. van der Wal, and S. Lloyd, Science **285**, 1036 (1999).
[3] J. Koch, T. M. Yu, J. Gambetta, A. A. Houck, D. I. Schuster, J. Majer, A. Blais, M. H. Devoret, S. M. Girvin, and R. J. Schoelkopf, Phys. Rev. A **76**, 042319 (2007).
[4] F. Arute *et al.*, Nature (London) **574**, 505 (2019).
[5] Google Quantum AI, Nature (London) **595**, 383 (2021).
[6] A. Kandala, A. Mezzacapo, K. Temme, M. Takita, M. Brink, J. M. Chow, and J. M. Gambetta, Nature (London) **549**, 242 (2017).
[7] F. Motzoi, J. M. Gambetta, P. Rebentrost, and F. K. Wilhelm, Phys. Rev. Lett. **103**, 110501 (2009).
[8] V. Negîrneac, H. Ali, N. Muthusubramanian, F. Battistel, R. Sagastizabal, M. S. Moreira, J. F. Marques, W. J. Vlothuizen, M. Beekman, C. Zachariadis, N. Haider, A. Bruno, and L. DiCarlo, Phys. Rev. Lett. **126**, 220502 (2021).
[9] C. Chamberland, G. Zhu, T. J. Yoder, J. B. Hertzberg, and A. W. Cross, Phys. Rev. X **10**, 011022 (2020).
[10] J. B. Hertzberg, E. J. Zhang, S. Rosenblatt, E. Magesan, J. A. Smolin, J.-B. Yau, V. P. Adiga, M. Sandberg, M. Brink, J. M. Chow, and J. S. Orcutt, npj Quantum Inf. **7**, 129 (2021).
[11] B. M. Varbanov, F. Battistel, B. M. Tarasinski, V. P. Ostroukh, T. E. O'Brien, L. DiCarlo, and B. M. Terhal, npj Quantum Inf. **6**, 102 (2020).
[12] M. McEwen *et al.*, Nat. Commun. **12**, 1761 (2021).
[13] R. Barends, J. Kelly, A. Megrant, D. Sank, E. Jeffrey, Y. Chen, Y. Yin, B. Chiaro, J. Mutus, C. Neill, P. O'Malley, P. Roushan, J. Wenner, T. C. White, A. N. Cleland, and J. M. Martinis, Phys. Rev. Lett. **111**, 080502 (2013).
[14] C. Wang, C. Axline, Y. Y. Gao, T. Brecht, Y. Chu, L. Frunzio, M. H. Devoret, and R. J. Schoelkopf, Appl. Phys. Lett. **107**, 162601 (2015).
[15] N. P. de Leon, K. M. Itoh, D. Kim, K. K. Mehta, T. E. Northup, H. Paik, B. S. Palmer, N. Samarth, S. Sangtawesin, and D. W. Steuerman, Science **372**, eabb2823 (2021).
[16] V. E. Manucharyan, J. Koch, L. I. Glazman, and M. H. Devoret, Science **326**, 113 (2009).
[17] L. B. Nguyen, Y.-H. Lin, A. Somoroff, R. Mencia, N. Grabon, and V. E. Manucharyan, Phys. Rev. X **9**, 041041 (2019).
[18] H. Zhang, S. Chakram, T. Roy, N. Earnest, Y. Lu, Z. Huang, D. K. Weiss, J. Koch, and D. I. Schuster, Phys. Rev. X **11**, 011010 (2021).
[19] A. Somoroff, Q. Ficheux, R. A. Mencia, H. Xiong, R. V. Kuzmin, and V. E. Manucharyan, arXiv:2103.08578.
[20] A. P. M. Place *et al.*, Nat. Commun. **12**, 1779 (2021).
[21] C. Wang *et al.*, arXiv:2105.09890.
[22] Q. Ficheux, L. B. Nguyen, A. Somoroff, H. Xiong, K. N. Nesterov, M. G. Vavilov, and V. E. Manucharyan, Phys. Rev. X **11**, 021026 (2021).
[23] H. Xiong, Q. Ficheux, A. Somoroff, L. B. Nguyen, E. Dogan, D. Rosenstock, C. Wang, K. N. Nesterov, M. G. Vavilov, and V. E. Manucharyan, arXiv:2103.04491.

[24] L. DiCarlo, J. M. Chow, J. M. Gambetta, L. S. Bishop, B. R. Johnson, D. I. Schuster, J. Majer, A. Blais, L. Frunzio, S. M. Girvin, and R. J. Schoelkopf, Nature (London) **460**, 240 (2009).

[25] See Supplemental Material http://link.aps.org/supplemental/10.1103/PhysRevLett.129.010502, which includes Refs. [26–47] for additional details.

[26] J. M. Kreikebaum, K. P. O'Brien, A. Morvan, and I. Siddiqi, Supercond. Sci. Technol. **33**, 06LT02 (2020).

[27] A. Wallraff, D. I. Schuster, A. Blais, L. Frunzio, J. Majer, M. H. Devoret, S. M. Girvin, and R. J. Schoelkopf, Phys. Rev. Lett. **95**, 060501 (2005).

[28] P. V. Klimov *et al.*, Phys. Rev. Lett. **121**, 090502 (2018).

[29] M. Carroll, S. Rosenblatt, P. Jurcevic, I. Lauer, and A. Kandala, arXiv:2105.15201.

[30] G. Ithier, E. Collin, P. Joyez, P. J. Meeson, D. Vion, D. Esteve, F. Chiarello, A. Shnirman, Y. Makhlin, J. Schriefl, and G. Schön, Phys. Rev. B **72**, 134519 (2005).

[31] F. Yoshihara, K. Harrabi, A. O. Niskanen, Y. Nakamura, and J. S. Tsai, Phys. Rev. Lett. **97**, 167001 (2006).

[32] A. Kou, W. C. Smith, U. Vool, R. T. Brierley, H. Meier, L. Frunzio, S. M. Girvin, L. I. Glazman, and M. H. Devoret, Phys. Rev. X **7**, 031037 (2017).

[33] J. J. Burnett, A. Bengtsson, M. Scigliuzzo, D. Niepce, M. Kudra, P. Delsing, and J. Bylander, npj Quantum Inf. **5**, 54 (2019).

[34] Z. Chen *et al.*, Phys. Rev. Lett. **116**, 020501 (2016).

[35] S. Sheldon, L. S. Bishop, E. Magesan, S. Filipp, J. M. Chow, and J. M. Gambetta, Phys. Rev. A **93**, 012301 (2016).

[36] J. R. Johansson, P. D. Nation, and F. Nori, Comput. Phys. Commun. **183**, 1760 (2012).

[37] J. R. Johansson, P. D. Nation, and F. Nori, Comput. Phys. Commun. **184**, 1234 (2013).

[38] L. H. Pedersen, N. M. Møller, and K. Mølmer, Phys. Lett. A **367**, 47 (2007).

[39] M. A. Rol, L. Ciorciaro, F. K. Malinowski, B. M. Tarasinski, R. E. Sagastizabal, C. C. Bultink, Y. Salathe, N. Haandbaek, J. Sedivy, and L. DiCarlo, Appl. Phys. Lett. **116**, 054001 (2020).

[40] M. A. Rol, F. Battistel, F. K. Malinowski, C. C. Bultink, B. M. Tarasinski, R. Vollmer, N. Haider, N. Muthusubramanian, A. Bruno, B. M. Terhal, and L. DiCarlo, Phys. Rev. Lett. **123**, 120502 (2019).

[41] D. C. McKay, C. J. Wood, S. Sheldon, J. M. Chow, and J. M. Gambetta, Phys. Rev. A **96**, 022330 (2017).

[42] M. Horodecki, P. Horodecki, and R. Horodecki, Phys. Rev. A **60**, 1888 (1999).

[43] M. A. Nielsen, Phys. Lett. A **303**, 249 (2002).

[44] K. N. Nesterov, I. V. Pechenezhskiy, C. Wang, V. E. Manucharyan, and M. G. Vavilov, Phys. Rev. A **98**, 030301(R) (2018).

[45] P. J. J. O'Malley *et al.*, Phys. Rev. Applied **3**, 044009 (2015).

[46] A. D. Córcoles, J. M. Gambetta, J. M. Chow, J. A. Smolin, M. Ware, J. Strand, B. L. Plourde, and M. Steffen, Phys. Rev. A **87**, 030301(R) (2013).

[47] N. Schuch and J. Siewert, Phys. Rev. A **67**, 032301 (2003).

[48] R. Barends *et al.*, Nature (London) **508**, 500 (2014).

[49] A. Blais, A. L. Grimsmo, S. M. Girvin, and A. Wallraff, Rev. Mod. Phys. **93**, 025005 (2021).

[50] V. E. Manucharyan, J. Koch, M. Brink, L. I. Glazman, and M. H. Devoret, arXiv:0910.3039.

[51] D. Gusenkova, M. Spiecker, R. Gebauer, M. Willsch, D. Willsch, F. Valenti, N. Karcher, L. Grünhaupt, I. Takmakov, P. Winkel, D. Rieger, A. V. Ustinov, N. Roch, W. Wernsdorfer, K. Michielsen, O. Sander, and I. M. Pop, Phys. Rev. Applied **15**, 064030 (2021).

[52] E. Knill, D. Leibfried, R. Reichle, J. Britton, R. B. Blakestad, J. D. Jost, C. Langer, R. Ozeri, S. Seidelin, and D. J. Wineland, Phys. Rev. A **77**, 012307 (2008).

[53] E. Magesan, J. M. Gambetta, and J. Emerson, Phys. Rev. Lett. **106**, 180504 (2011).

[54] E. Magesan, J. M. Gambetta, B. R. Johnson, C. A. Ryan, J. M. Chow, S. T. Merkel, M. P. da Silva, G. A. Keefe, M. B. Rothwell, T. A. Ohki, M. B. Ketchen, and M. Steffen, Phys. Rev. Lett. **109**, 080505 (2012).

[55] S. Gustavsson, O. Zwier, J. Bylander, F. Yan, F. Yoshihara, Y. Nakamura, T. P. Orlando, and W. D. Oliver, Phys. Rev. Lett. **110**, 040502 (2013).

[56] Y. Sung, L. Ding, J. Braumüller, A. Vepsäläinen, B. Kannan, M. Kjaergaard, A. Greene, G. O. Samach, C. McNally, D. Kim, A. Melville, B. M. Niedzielski, M. E. Schwartz, J. L. Yoder, T. P. Orlando, S. Gustavsson, and W. D. Oliver, Phys. Rev. X **11**, 021058 (2021).

[57] P. Zhao, P. Xu, D. Lan, J. Chu, X. Tan, H. Yu, and Y. Yu, Phys. Rev. Lett. **125**, 200503 (2020).

[58] J. Stehlik, D. M. Zajac, D. L. Underwood, T. Phung, J. Blair, S. Carnevale, D. Klaus, G. A. Keefe, A. Carniol, M. Kumph, M. Steffen, and O. E. Dial, Phys. Rev. Lett. **127**, 080505 (2021).

[59] D. P. DiVincenzo, Fortschr. Phys. **48**, 771 (2000).

[60] Y. Wu *et al.*, Phys. Rev. Lett. **127**, 180501 (2021).

[61] R. Harris, A. J. Berkley, M. W. Johnson, P. Bunyk, S. Govorkov, M. C. Thom, S. Uchaikin, A. B. Wilson, J. Chung, E. Holtham, J. D. Biamonte, A. Y. Smirnov, M. H. S. Amin, and A. Maassen van den Brink, Phys. Rev. Lett. **98**, 177001 (2007).

[62] A. O. Niskanen, K. Harrabi, F. Yoshihara, Y. Nakamura, S. Lloyd, and J. S. Tsai, Science **316**, 723 (2007).

[63] D. Rosenberg, D. Kim, R. Das, D. Yost, S. Gustavsson, D. Hover, P. Krantz, A. Melville, L. Racz, G. O. Samach, S. J. Weber, F. Yan, J. L. Yoder, A. J. Kerman, and W. D. Oliver, npj Quantum Inf. **3**, 42 (2017).